



**HAL**  
open science

## CFD analysis of the flow in the MICAS experimental facility, a water model of the hot pool of a sodium cooled fast reactor

U. Bieder, J. Maillard, Y. Gorsse, D. Guenadou

► **To cite this version:**

U. Bieder, J. Maillard, Y. Gorsse, D. Guenadou. CFD analysis of the flow in the MICAS experimental facility, a water model of the hot pool of a sodium cooled fast reactor. Nuclear Engineering and Design, 2019, 350, pp.67-77. 10.1016/j.nucengdes.2019.04.033 . cea-02529676

**HAL Id: cea-02529676**

**<https://cea.hal.science/cea-02529676>**

Submitted on 22 Oct 2021

**HAL** is a multi-disciplinary open access archive for the deposit and dissemination of scientific research documents, whether they are published or not. The documents may come from teaching and research institutions in France or abroad, or from public or private research centers.

L'archive ouverte pluridisciplinaire **HAL**, est destinée au dépôt et à la diffusion de documents scientifiques de niveau recherche, publiés ou non, émanant des établissements d'enseignement et de recherche français ou étrangers, des laboratoires publics ou privés.



Distributed under a Creative Commons Attribution - NonCommercial 4.0 International License

## CFD ANALYSIS OF THE FLOW IN THE MICAS EXPERIMENTAL FACILITY, A WATER MODEL OF THE HOT POOL OF A SODIUM COOLED FAST REACTOR

U. Bieder<sup>1</sup>, J. Maillard<sup>1</sup>, Y. Gorsse<sup>1</sup>, D. Guenadou<sup>2</sup>

<sup>1</sup> DEN-STMF, CEA, Université Paris-Saclay, F-91191 Gif-sur-Yvette, France

<sup>2</sup> CEA Cadarache, DTN/STCP/LHC, F-13108 Saint Paul lez Durance, France

### Abstract

Sodium Cooled Fast Reactors (SFRs) have been developed in France for about 50 years including the research reactors Rapsodie and Phenix as well as the Superphenix plant. In the framework of Generation IV reactor deployment, the development the Advanced Sodium Technological Reactor for Industrial Demonstration (ASTRID) was started in 2006 under the leadership of CEA. Current activities on the use of Computational Fluid Dynamics (CFD) in the ASTRID project are focused on the validation of computational tools to predict the thermal-hydraulic behavior of sodium in the reactor vessel. As thermal hydraulics is recognized as key scientific subject in the development of SFRs, new experiments are realized for both qualification of design options and validation of code calculations. Large scale tests are conducted in water models such as the MICAS facility, which represents the hot pool of the ASTRID reactor in 1/6 scale including all internals. The facility is built in transparent polymer for accurate optical measurements of the flow field under various flow conditions.

The flow in the MICAS facility is analyzed with the CEA in-house code TrioCFD, the reference CFD code of the Nuclear Reactor Division of the CEA. The use of HPC (High Performance Computing) allows the access to flow fields in complex geometrical structures with a high resolution in time and space. The validation of the modelling approach is shown on the example of the MICAS experiment by comparing calculation results (velocity fields) to LDV measurements. Detailed information is given on the test facility, the used modelling approach and the comparison between experiment and calculation. Although the calculation is globally in accordance to the experiment, differences exist locally due to the complexity of the flow topology in the hot pool.

### 1. INTRODUCTION

Sodium cooled Fast Reactors (SFRs) have been developed in France for about 50 years including the construction of the research reactors Rapsodie and Phenix as well as of the Superphenix plant (Tenchine et al. 2010). In the framework of Generation IV reactor deployment, the development of the “Advanced Sodium Technological Reactor for Industrial Demonstration” (ASTRID) was announced in 2006 (Dufour, 2013). Thermal hydraulics is recognized as a key scientific subject in the development of SFRs. This paper deals with the development and validation of CFD models to predict the flow field in the upper plenum of pool type SFRs in general and of the ASTRID reactor in particular (Alphonse, 2013).

Various SFR related integral experiments in large-scale water models were performed in the past. For the Superphenix reactor, a 1/15 scale, 360° model of the upper plenum (also called hot pool) was build and operated in the late 1970<sup>th</sup> for thermal hydraulic analyses. Grand et al, (1979) presented for this facility a detailed scaling study, preliminary velocity measurements and first results with CFD. CEA build in the early 1990<sup>th</sup> a 90°sector facility at a reduced scale of 1/5 of Superphenix reactor upper plenum for studying the thermal hydraulic behavior of both core outlet region and upper plenum (Tenchine et al., 2010). Effects of the inter-wrapper region (gaps between the assemblies) on the flow behavior in the hot pool were not taken into account in this facility. Thus, a new water facility for studying the core outlet region of the European Fast Reactor was built at CEA in the mid 1990<sup>th</sup> with a representation of the inter-wrapper region (Tenchine et al., 2010). This facility represented a sector of 90° at a reduced scale of 1/3.

The facility allowed studying the recirculating flow in the upper plenum and its influence on the core outlet behavior.

Within the European Fast Breeder Reactor Project, an experimental approach in the RAMONA facility has been largely used to study decay heat removal situations (Hoffmann, 1989). RAMONA was a 1/20 scale water model of the upper plenum with boundary conditions imposed at the core outlet and with active immersed coolers. Transient situations were tested and the interaction between cold Sodium flowing downwards from the coolers and hot Sodium flowing upwards from the core was analyzed in detail. A larger water model at a 1/5 scale, called NEPTUN, was also used to estimate the scale effect on the results for a better extrapolation to the reactor (Weinberg, 1996).

The IAEA has coordinated a research project (CRP) between 2008 and 2012 entitled “Benchmark Analysis of Sodium Natural Convection in the Upper Plenum of the MONJU Reactor Vessel” (IAEA, 2014). Japan Atomic Energy Agency (JAEA) has submitted to the CRP participants the data of Sodium thermal stratification measurements in the in MONJU reactor vessel Upper Plenum, collected during a plant trip test conducted in December 1995. The benchmark partners have analyzed this experiment by applying different codes and methodologies (Ohira et al, 2013). The benchmark thus helped the members to improve their capability in the field of fast reactor in-vessel Sodium thermal hydraulics (Bieder et al., 2013).

An integrated, thermal hydraulic, CFD based simulation of primary sodium system and safety grade decay heat removal system has been carried out by Rajamani et al. (2016) to assess the role of inter-wrapper flow in decay heat removal under complete station black out condition, in a medium size 1250 MW thermal pool type sodium cooled fast reactor. Rahhi et al. (2017) carried out a detailed integrated CFD investigation of heat transfer enhancement with multi-tray core catcher. The evolution of transient temperature at critical locations in the structure and maximum temperature in core debris was studied to assess the structural integrity of the core catcher trays of a typical 500 MWe SFR.

Gerschenfeldt et al (2017) showed that local flow phenomena in SFR reactors might have a strong feedback effect on the global behavior of the reactor. Therefore, algorithms for coupling a system code (CATHARE), a component code (TrioMC) and a CFD code (TrioCFD) were developed. The code system was validated by analyzing PLANDTL-DHX tests that were performed at the Japan Atomic Energy Agency.

## **2. THE ASTRID REACTOR**

The generation IV ASTRID reactor is based on the concept of a pool type sodium cooled fast breeder reactor. Such a reactor is shown schematically on the left of Fig.1. Cold sodium from the cold pool is drawn into the main coolant pump and driven into the reactor core. Absorbing the heat from the fissile core the hot sodium is then injected into the hot pool. A scheme of the flow in the hot pool is shown on the left side of Fig.1. The hot sodium is leaving the core in form of multiple jets. These jets combine and divide into two main flow paths. A minor part of the flow is entering the upper core structure (UCS), a geometrically complex structure formed by control rods and instrumentation tubes, which are enclosed by a cylinder perforated by holes. As the UCS presents a significant flow resistance, the major part of the flow is deflected by the UCS and is entering the hot pool in form of an inclined plane jet. This jet is disturbed in azimuthal direction by the control rods present in the space between core exit and UCS entry.

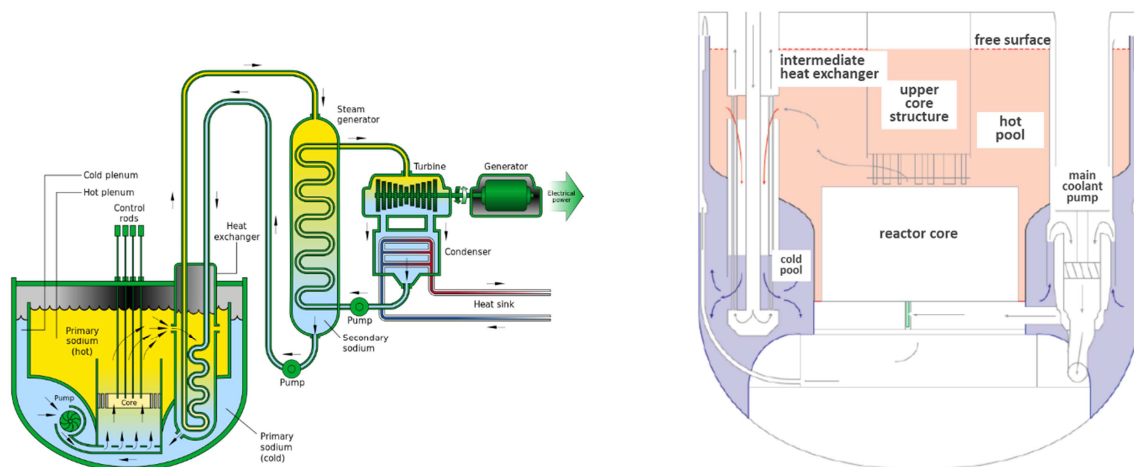


Fig. 1: Scheme of a pool type SFR (left side) and zoom on the upper plenum (right side)

After having traversed the large volume of the hot pool, hot sodium is transported into the intermediate heat exchangers (IHX), which are disposed in a non-symmetrical way along the periphery of the hot pool. The hot sodium is cooled down in the IHX by the sodium of the secondary circuit. Then, the sodium is transported by natural convection into the cold pool.

The described flow in the hot pool is highly turbulent, momentum driven and influenced by buoyancy. The prediction of this flow on reactor scale by CFD demands significant validation work including new experiments. The operation of the MICAS facility under various flow conditions and the analysis of the deduced data by CFD represent an important contribution to the qualification of CFD models for ASTRID applications. The evaluation of such a calculation methodology is subject of this paper.

### 3. THE MICAS FACILITY

The flow field in the hot plenum of SFRs is highly complex involving jet- and recirculating zones where the sodium flows at velocities, which are significantly lower than main stream velocities near the core outlet. In order to understand this complex flow better, the MICAS test facility (French acronym for “hot pool test facility for ASTRID”) is operated at CEA-Cadarache. MICAS is a 1/6 scale mock-up operated with water, geometrically similar to the ASTRID hot pool (Guenadou et al, 2015 and Guenadou et al, 2016). A perspective view from above into the facility is given on the left side of Fig.2. The locations of the three main coolant pumps (PO1-PO3), the four intermediate heat exchangers (IHX1-IHX4) and the four direct heat exchangers (DHX1-DHX4) are given in the top view on the right side. Most of the components are built in transparent Poly-methyl-methacrylate polymer (PMMA) for optical visualizations. The scale was chosen as a compromise between the overall size and the detail of the geometry of the vessel. Due to high mechanical stresses, some specific components were manufactured in aluminum: upper part of the core (high pressure in the injection chamber), inlet of the intermediate heat exchangers IHX1 to IHX4 (thin and soaring structure) and the bottom grid of the UCS (very high porosity).

The MICAS core simulant is split in three outlet regions to represent the ASTRID design: the fission area, the reflectors and the internal fuel storage region. The flow rate in each zone is controlled according to the real flow distribution in the ASTRID reactor. The following quantities are measured during the first hydraulic measuring campaign (Guenadou et al, 2017):

- Velocity fields in various vertical plans in the hot pool (particularly around UCS and IHX) by using PIV techniques. The acquisition rate is 15 Hz (integration time is 10 s). The error of the

measured velocities has been evaluated to be about 1%. The laser planes are positioned with an error of  $\pm 1^\circ$ .

- Water injection flow rates in the three core regions, measured by three Coriolis flowmeters with an accuracy of 0.1%;
- Location of the water level above the core outlet plate, measured with an accuracy of  $\pm 2$  mm;
- Flow rate entering the UCS measured by integrating the measured velocity fields along the inlet of the UCS as well as at the UCS barrel holes (accuracy below 10%).

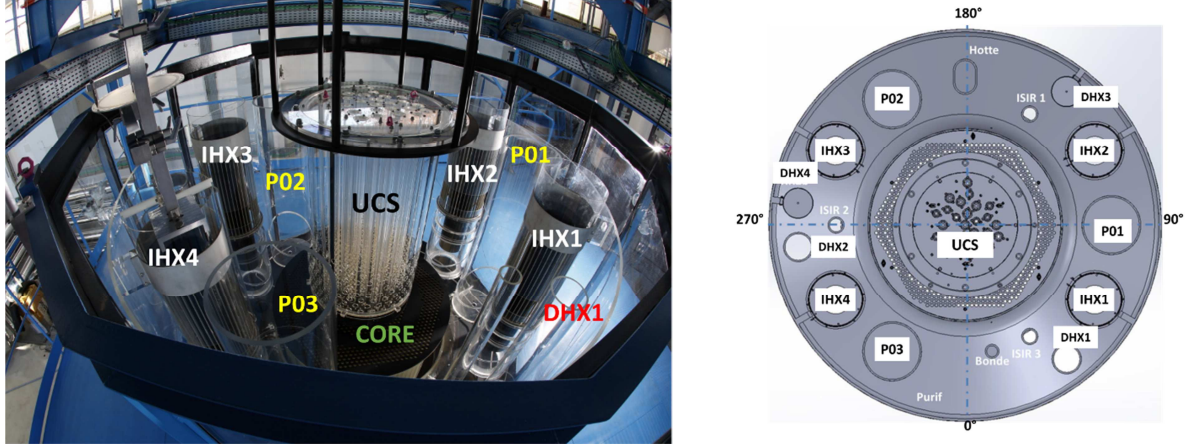


Fig. 2: The MICAS facility; perspective view on the left side, location of the internals on the right side

#### 4. MODELLING OF THE MICAS FACILITY

Water is assumed to be Newtonian and incompressible. As only isothermal experiments are discussed in this paper, buoyancy effects are not taken into account. The instantaneous velocity  $u$  of such a fluid can be expressed by the equation of mass conservation Eq.1 and momentum conservation Eq.2 (Pope, 2000). Einstein's matrix notation is used.

$$\frac{\partial u_j}{\partial x_j} = 0 \quad (1)$$

$$\frac{\partial u_i}{\partial t} + \frac{\partial (u_i u_j)}{\partial x_j} = -\frac{1}{\rho} \frac{\partial p}{\partial x_i} + \frac{\partial}{\partial x_j} \left[ \nu_{eff} \left( \frac{\partial u_i}{\partial x_j} + \frac{\partial u_j}{\partial x_i} \right) \right] + \frac{S_{M,i}}{\rho} \quad (2)$$

For laminar flow, the effective viscosity  $\nu_{eff}$  is the kinematic viscosity  $\nu$  of the fluid.  $S_M$  is a momentum source term to account for the effect of singular or directional pressure losses.

##### 4.1 Turbulence treatment

In Reynolds-averaged approaches to turbulence, the non-linearity of the Navier-Stokes equations gives rise to Reynolds stress terms that are modelled by turbulence models. Boussinesq's eddy-viscosity concept assumes that (Pope, 2000):

$$-\overline{u'_i u'_j} \equiv \nu_t \left( \frac{\partial U_i}{\partial x_j} + \frac{\partial U_j}{\partial x_i} \right) - \frac{2}{3} k \delta_{ij} \quad (3)$$

$U_i$  represents the component in  $i$ -direction of the Reynolds averaged velocity. The averaging approach leads to the Reynolds averaged Navier-Stokes equations (RANS). Eq.2 is then written for  $U_i$  and  $\nu_{eff} = \nu + \nu_t$ . The turbulent viscosity  $\nu_t$  is calculated here from the well-known  $k$ - $\epsilon$  model ( $k$  is the turbulent kinetic

energy and  $\varepsilon$  its dissipation). A weakness of this model is related to the fact that  $\nu_t$  is assumed being an isotropic scalar quantity. This hypothesis prevents the model of treating anisotropic turbulence as impinging jets, rotational flow and flow curvature. Such flow features are present in the hot pool of SFRs. However, the objective of this study is to evaluate a modelling methodology, which can be applied to MICAS and later to longer reactor transients of ASTRID. Therefore, important calculation time consuming turbulence models such as *Reynolds Stress Models* or *Large Eddy Simulations* have been excluded from the study. Just as well, *Non-Linear Eddy Viscosity Models* have been excluded from the study as a physically correct representation of all flow phenomena in the hot pool of ASTRID cannot be guaranteed by this model-family. **In fact, Bieder (2012) has shown for rod bundles that *Non-linear eddy viscosity models* can lead to wrong results for secondary flows, which are created by anisotropic turbulence. Nevertheless, an improvement of the actual turbulence modelling strategy is planned for future studies.**

The following formulation of the k- $\varepsilon$  model is used (Pope, 2000):

$$v_t = c_\mu \frac{k}{\varepsilon} \quad (4)$$

$$\frac{\partial k}{\partial t} + \frac{\partial(U_j k)}{\partial x_j} = \frac{\partial}{\partial x_j} \left[ \left( \nu + \frac{\nu_t}{\sigma_k} \right) \frac{\partial k}{\partial x_j} \right] - \varepsilon + P \quad (5)$$

$$\frac{\partial \varepsilon}{\partial t} + \frac{\partial(U_j \varepsilon)}{\partial x_j} = \frac{\partial}{\partial x_j} \left[ \left( \nu + \frac{\nu_t}{\sigma_\varepsilon} \right) \frac{\partial \varepsilon}{\partial x_j} \right] + C_{\varepsilon 1} P \frac{\varepsilon}{k} - C_{\varepsilon 2} \frac{\varepsilon^2}{k} \quad (6)$$

$$P = -\overline{u'_i u'_j} \frac{\partial U_i}{\partial x_j} \quad (7)$$

The Reynolds stresses  $\overline{u'_i u'_j}$  are calculated from Eq.3. The following empirical coefficients are used:  $c_\mu=0.09$ ,  $\sigma_k=1$ ,  $\sigma_\varepsilon=1.3$ ,  $C_{\varepsilon 1}=1.44$ ,  $C_{\varepsilon 2}=1.92$ .

## 4.2 Geometrical model and meshing of the MICAS facility

Based on multi-year experience in modelling integral tests in water as the ROCOM facility (Feng et al., 2017, Höhne et al., 2018) or in sodium as the SUPERCAVNA facility (Bieder et al, 2018), Best Practice Guidelines (BPG) have been defined for TrioCFD<sup>1</sup> applications to experiments like MICAS. The following description of the numerical model is based on these guidelines concerning CAD model, meshing, numerical schemes, boundary conditions and solution method.

In order to achieve convergence of the calculated flow field on mesh refinement both the geometrical model and the meshing of the MICAS facility have been optimized step by step. For this purpose, PYTHON scrips have been developed for SALOME<sup>2</sup> platform. The CAD model has been improved successively and designed more and more realistically. The use of pressure loss correlations to represent small geometrical features of the facility has been avoided where possible. In a similar way, the necessary mesh refinement was achieved successively:

- **The coarsest tested meshes contained about  $5 \times 10^6$  tetrahedrons. Steady state solution was never achieved with this mesh, even with now order numerical schemes. The flow fluctuated temporally in large parts of the test facility.**

<sup>1</sup> <http://www-trio-u.cea.fr/>

<sup>2</sup> <https://www.salome-platform.org/>

- Several test calculations with medium size meshes of about  $15 \times 10^6$  tetrahedrons were performed by using local mesh refinement techniques. These calculations did lead neither to steady state solutions in the wake of the heat exchangers nor to results that are independent of the localization of the zones with mesh refinement.
- A fine meshing of  $28 \times 10^6$  tetrahedrons of similar size and angles of about  $60^\circ$  between the faces of the tetrahedrons was finally retained for the analysis. Steady state solutions were achieved in the locations of the measurements. Specific treatment of the near wall meshing by introducing prismatic cells was tested. The comparison of calculations with and without prismatic cells did not show a significant influence of the near wall meshing on the overall flow field, as the geometry of the test facility (heat exchangers, bottom grid and UCS) predominantly influences the flow and not the formation of boundary layers on walls.

Further refinement of the mesh did not significantly modify the resulting overall flow field. The resulting geometrical model and this fine mesh is shown in Fig.3 on the example of a vertical plane, cut for an azimuthal angle of  $54^\circ$  through IHX1 and IHX3. Solid walls are shown as red lines. The flow holes in the UCS are explicitly meshed with about **seven calculation points per hole diameter**. Very small geometrical features are modeled by singular pressure losses. Their locations are shown as green lines: the bottom grid (circular perforated plate), the perforated section of the guide tubes and the inlet structures of the IHXs. Singular pressure losses are taken into account in the Navier-Stokes equations Eq.2 as momentum source terms  $S_M$  and are defined as:

$$\frac{S_{M,i}}{\rho} = \frac{\Delta p}{\rho} = \frac{1}{2} \cdot K_i \cdot |U| \cdot U_i \vec{n} \quad (8)$$

$K_i$  is the directional singular pressure loss coefficient and  $\vec{n}$  the normal vector of the perforated surfaces. The pressure loss coefficients were taken from Idel'Chik, 1986:  $K_i = (0 \ 0 \ 4.8)^T$  for the bottom grid,  $K_i = (54 \ 54 \ 54)^T$  for the guide tubes and  $K_i = (0.5 \ 0.5 \ 0.1)^T$  for the IHX. The reduction of the flow area in the guide tubes due to the presence of control rods is modeled by means of porosities (blue zones in Fig. 3) and singular pressure losses at the inlet of the guide tubes in order to simulate the resulting sudden contraction of the flow area.

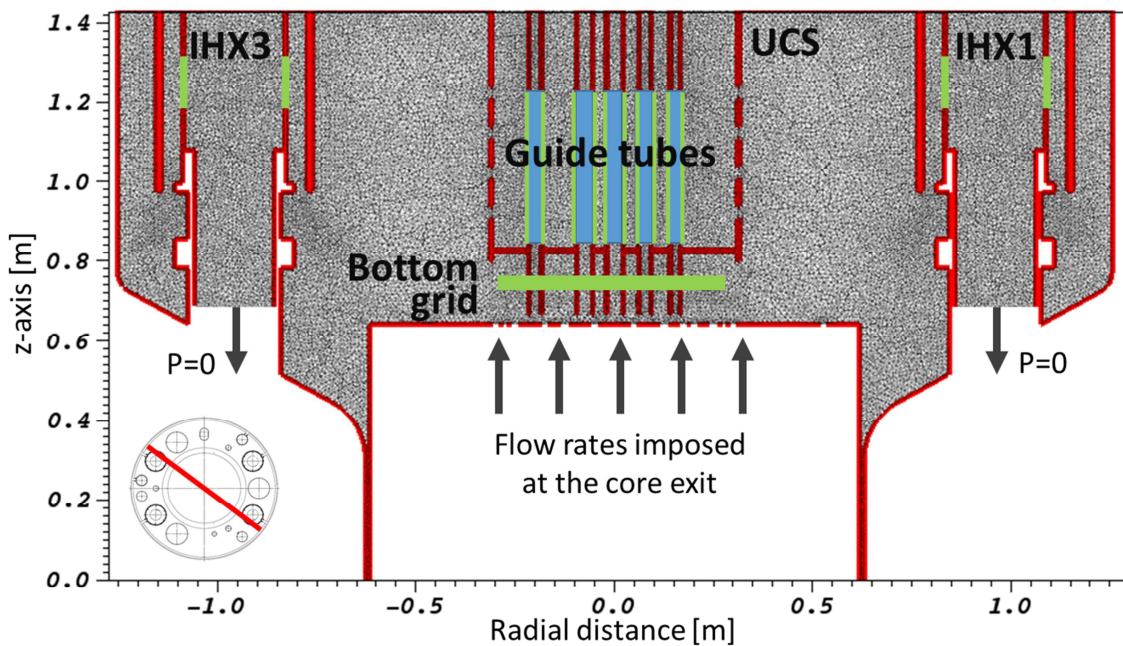


Fig.3: Meshing and modelling of the upper core structure

### 4.3 Physical properties and boundary conditions

Physical properties of water have been taken for 22°C and are assumed to be constant. Dirichlet boundary conditions were used at the core exit (core plate) for velocity,  $k$  and  $\varepsilon$ . For each assembly outlet, constant values of the mean velocity as well as of  $k$  and  $\varepsilon$  were imposed. In this context,  $k$  and  $\varepsilon$  were calculated from the spatial mean core outlet velocity  $|U_c|$  and the hydraulic diameter of the assembly outlet  $d_h$  (Beck et al. 2017), assuming a turbulence level of 10%:

$$k = \frac{1}{2} \cdot (u')^2, \quad \varepsilon = \frac{c_\mu^{3/4} \cdot k^{3/2}}{d_h} \quad \text{and} \quad u' \approx 0.1 \cdot |U_c|. \quad (9)$$

Neumann boundary conditions are applied at the outflow faces of the four IHXs with an imposed constant pressure for the momentum equations (same pressure at all IHXs) and free outflow conditions for  $k$  and  $\varepsilon$ . The water surface is modeled as free-slip wall. Wall functions are used to model momentum exchange between walls and fluid. **The general wall law of Reichardt (Reichardt, 1952) is used, which is written for non-dimensional values of wall distance ( $y^+$ ) and velocity ( $U^+$ ):**

$$U^+ = \frac{U}{U_\tau} = \frac{1}{\kappa} \ln(1 + \kappa y^+) + 7.8 \left( 1 - e^{\left(\frac{-y^+}{11}\right)} - \frac{y^+}{11} e^{\left(\frac{-y^+}{3}\right)} \right) \quad (10)$$

$U_\tau$  is the friction velocity. Reichardt' law is a blending function that spans the whole wall boundary layer from the wall ( $U^+ = 0$ ), where it matches the viscous sub layer closely, over the buffer region to the logarithmic sublayer, where it converges asymptotely to the logarithmic wall law ( $U^+ = \ln(y^+)/\kappa + 5.1$ ). Local equilibrium between production and dissipation of turbulent kinetic energy is assumed at the first near wall calculation point. The following boundary conditions for  $k$  and  $\varepsilon$  are derived from Reichardt's wall law (Eq.10). The functions are written in non-dimensional form:

$$k^+ = \frac{k}{U_\tau^2} = 0.07 \cdot y^{+2} \cdot e^{\left(\frac{-y^+}{9}\right)} + \frac{1}{\sqrt{c_\mu}} \left( 1 - e^{\left(\frac{-y^+}{20}\right)} \right)^2 \quad (11)$$

$$\varepsilon^+ = \frac{\varepsilon}{\nu U_\tau^4} = \frac{1}{\kappa \cdot (y^{+2} + 15^4)^{\frac{1}{4}}} \quad (12)$$

**For the fine mesh with  $28 \times 10^6$  tetrahedrons, the non-dimensional wall distance  $y^+$  is about 30 on the outer wall of the hot pool vessel. The  $y^+$  value is distributed non-homogeneously on the walls of flow obstacles as heat exchangers (IHXs and DHXs) and pumps (POs). In fact,  $y^+$  is about 100 in the zones where the jet leaving the core flows against obstacle walls and below 30 in the wake of the obstacles.**

### 4.4 Discretization and solution procedure

All calculations presented here have been performed with the CFD code TrioCFD (Angeli et al. 2015). The code is dedicated to unsteady, low Mach number, turbulent flows and is especially designed for industrial CFD calculations on tetrahedral grids of up to several hundreds of millions of meshes. TrioCFD is running on a daily basis on up to 10,000 processor cores of massively parallel computers.

A hybrid Finite Volume Element discretization method is implemented, which approximates a continuous problem by a discrete solution in the space of the finite elements by maintaining the balance notation of finite volumes. As in the classical element of Crouzieux and Raviart, (1973) the main vector- and scalar unknowns are located in the center of the faces of the tetrahedral element. The pressure is discretized in the center of an element and as extension of the classical element also in its vertices (Angeli et al 2017).

The resulting staggered mesh arrangement improves the velocity/pressure coupling, increases the divergence free basis and shows a hyper convergence behavior on mesh refinement. The SOLA velocity projection method (Hirt, 1975) is used to assure mass conservation.

In order to reach a steady state solution, a transient is calculated until the maximal variation of all quantities from one time step to another is below  $10^{-7}$  at all locations in the upper plenum. The time integration is performed by a fully implicit 1<sup>st</sup> order backward Euler scheme. It was assured by test calculations that the used time step of about  $10^{-3}$  s, which is ten times larger than that imposed by the Courant-Friedrich-Levy criterion (CFL=10), leads to the same steady state solution as for CFL=1. To stabilize numerically the calculation, a 1<sup>st</sup> order upwind convection scheme is used during the transient to steady state. Increasing the order of the convection scheme does not alter the achieved steady state solution in the regions of interest. This was assessed by various restarts from steady state and replacing the 1<sup>st</sup> order upwind scheme by 2<sup>nd</sup> order *muscl* type and *finite element based* convection schemes (Ducros et al. 2010). Finally, to complete the description of the numerical scheme, the diffusion term is discretized by a centered 2<sup>nd</sup> order method.

## 5. ANALYSIS OF A MICAS MIXING EXPERIMENT

The analyzed experiment was performed with a total flow rate of  $371.8 \text{ m}^3/\text{h}$ . The flow is distributed at the core exit according to 95.5 % in the fissile zone, 1.1 % in the reflector zone and 3.4% in the storage zone (Beck et al. 2017). The water level is stable at the height 0.786 m above the core plate ( $z=1.425 \text{ m}$ ). Initial condition is a stagnant velocity field ( $\vec{U} = 0$ ). The steady state solution is achieved numerically after a transient of about 45 s and experimentally after a few minutes (Guenadou et al. 2017).

### 5.1 Qualitative description of the flow field

Features of the calculated steady state flow field are shown for vertical and horizontal cut planes. It is interesting to see that the flow field is very complex with large circulation zones and jets entering the UCS. Fig. 4 shows the magnitude of the velocity (norm) in color scale and the corresponding velocity vectors indicate the direction of the flow. The visualization plane on the left side of Fig.4 is located below the UCS at  $z=0.675\text{m}$  (axial location see also Fig.3).

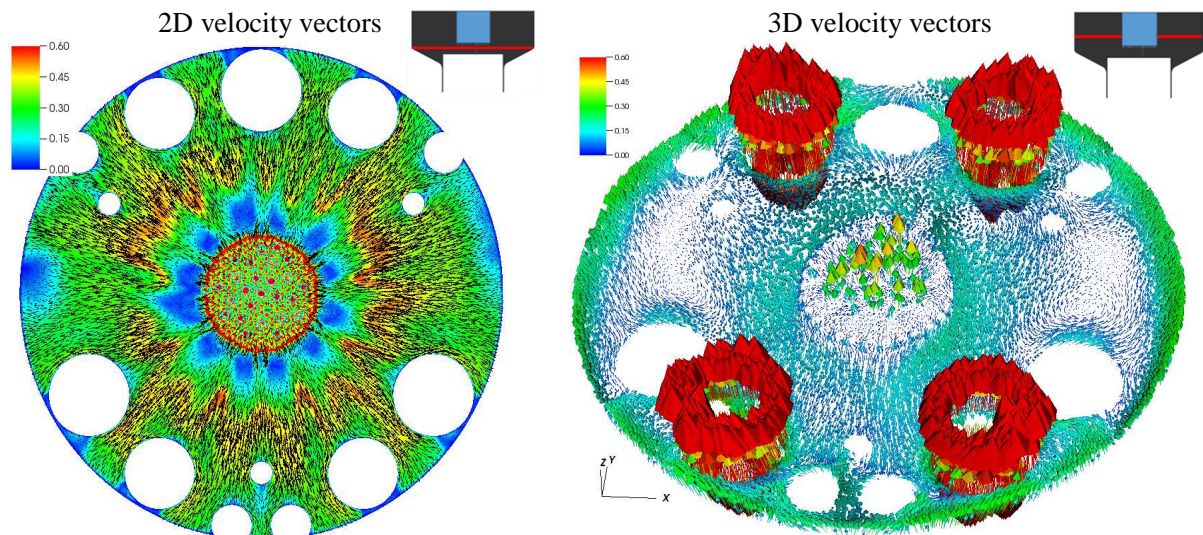


Fig.4: Horizontal planes: Norm of the velocity and velocity vectors below the UCS at  $z=0.675\text{m}$  (left) and in the UCS at  $z=0.975 \text{ m}$  (right)

The vectors are projected in the plane (2D vectors). The deflected horizontal jet is azimuthally not homogeneously distributed. In fact, the jet shows the formation of angle dependent zones with very different radial velocities due to the presence of guide tubes. On the right side of Fig.4 is shown the 3D vector field in perspective view for the plane  $z=0.975$  m inside the UCS. The flow in the guide tubes and in the UCS flow holes is visible as well as a large horizontal circulation in the region between UCS and IHXs. The velocity near the IHXs inlets is also not distributed equally around the IHX inlets.

Calculation results in vertical planes, cut at an azimuthal angle of  $54^\circ$  are shown in Figs.5 and 6. The counter clock wise orientation of the angles is defined in Fig.2. **The norm of the velocity and velocity vectors in the UCS, the space between UCS and IHX3 as well as in IHX3 are given on Fig.5. The flow leaves the core vertically and is deflected horizontally by the UCS. This effect is clearly visible in Fig.5 as well as the acceleration of the flow in the IHX. The flow develops a large circulating loop in the upper plenum, driven by the deflected jet.** Velocity vectors and pressure field near the UCS are given on Fig.6. The flow going into the UCS via the guide tubes is visible as well as the homogenization of the jets leaving the core and the already mentioned horizontal deflection of the flow. The pressure drop across the bottom of the UCS visible as well as the pressure drop across the barrel holes. The high pressure below the UCS deflects the flow horizontally.

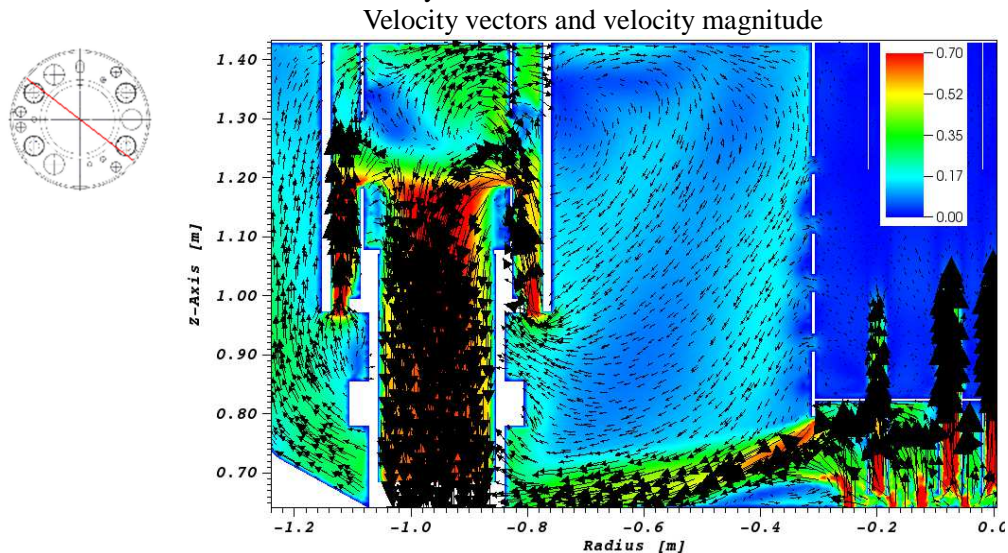


Fig.5: Vertical planes at  $54^\circ$ : Norm of the velocity and velocity vectors near the IHX3

Velocity vectors and pressure

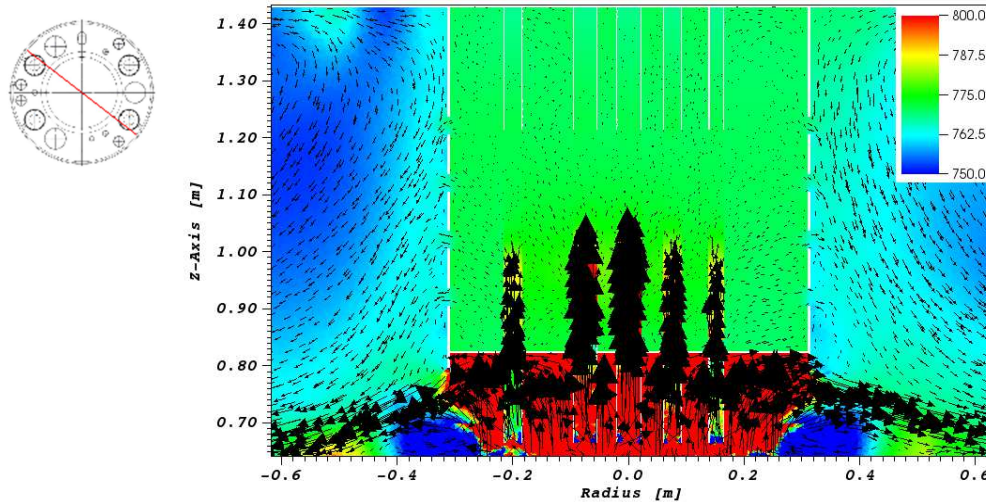


Fig.6: Vertical planes at 54°: Velocity vectors and pressure field near the UCS

## 5.2 Comparison to the experiment

Two quantitative comparisons of measurements and calculations are presented. First, the mass fluxes entering the UCS are analyzed and then velocity fields near the UCS and close to the IHX are discussed.

### 5.2.1 Comparison of mass fluxes

A first quantitative comparison between experiment and calculation is realized on the mass flux balance of the UCS. The flow rate entering the UCS has been determined experimentally with two methods by Guenadou (Guenadou et al, 2017):

1. Integrating the mass flow leaving the USC by the barrel holes over a significant number of holes and
2. Integrating the mass flow of the deflected jet azimuthally and subtracting this value from the known total inflow.

Experimentally, the first method led to  $0.0167 \text{ m}^3/\text{s}$  and the second one to  $0.0183 \text{ m}^3/\text{s}$ , respectively. The calculated flow rate is determined to  $0.0180 \text{ m}^3/\text{s}$ , what is very close to the experimental ones.

### 5.2.2 Comparison of velocity fields

Before comparing flow velocities that are measured in 2D planes to values that are calculated on unstructured tetrahedral meshes, comparable fields of the calculation are extracted. Then, calculated and measured velocities fields are compared for locations close to the UCS and locations close to the inlets of IHXs.

#### 5.2.2.1 Generation of comparable velocity fields

The PIV measurements generate temporally averaged fields of velocity vectors (10 s mean values with 15 Hz sampling time). These vectors are distributed homogeneously in the Laser beam plane and are aligned along this plane (2D vector plots). Such a velocity field is shown in Fig.7 on the left side. Additional information is given in this figure on the MICAS geometry close to the measuring plane. The vectors show the flow direction and the color scale shows the magnitude of the vectors. In order to create the corresponding vector plots from converge steady state 3D calculations on non-regularly arranged tetrahedral meshes, a 4-step post processing procedure has been developed and validated:

1. Definition of a 3D sub-domain, which encloses all tetrahedral cells connected to the chosen experimental plane.
2. Extraction of the 3D velocity vectors of the sub-domain from the whole calculation domain.
3. Projection of the 3D velocity vectors onto the surfaces of the tetrahedral cells. This leads to 2D velocity fields following the surfaces of the meshing (center of Fig.7).
4. Projection of the 2D velocity field in the experimental plane (right side of Fig.7).

The first two steps of the procedure are integrated in TrioCFD, the two projection steps are performed with PHYTON scripts based on SALOME.

Fig. 7 shows the successive convergency of the calculated 3D-velocity field to the measured 2D-field due to the described 4-step projection procedure. On the left side, the measured velocity field is shown. In the center, the calculated 3D-velocity field is visualized that is projected on the faces of the tetrahedral mesh of the sub-domain. Apparently, it is difficult to compare this field to the measurements. On the right side, the velocities, projected previously on the faces of the tetrahedrons, are projected afterwards onto the 2D-plane. It is good visible that only the velocity vectors projected onto the 2D-plane can be compared to the measurements.

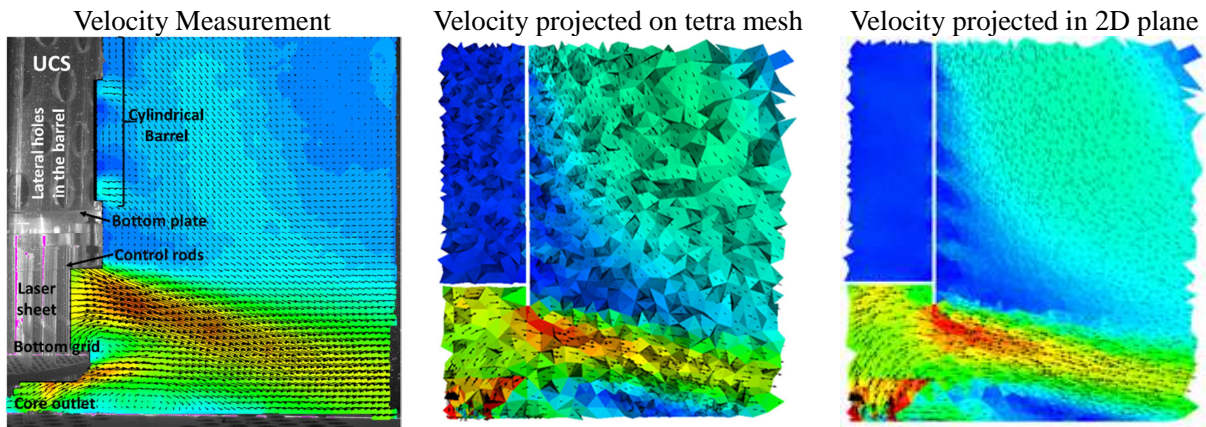


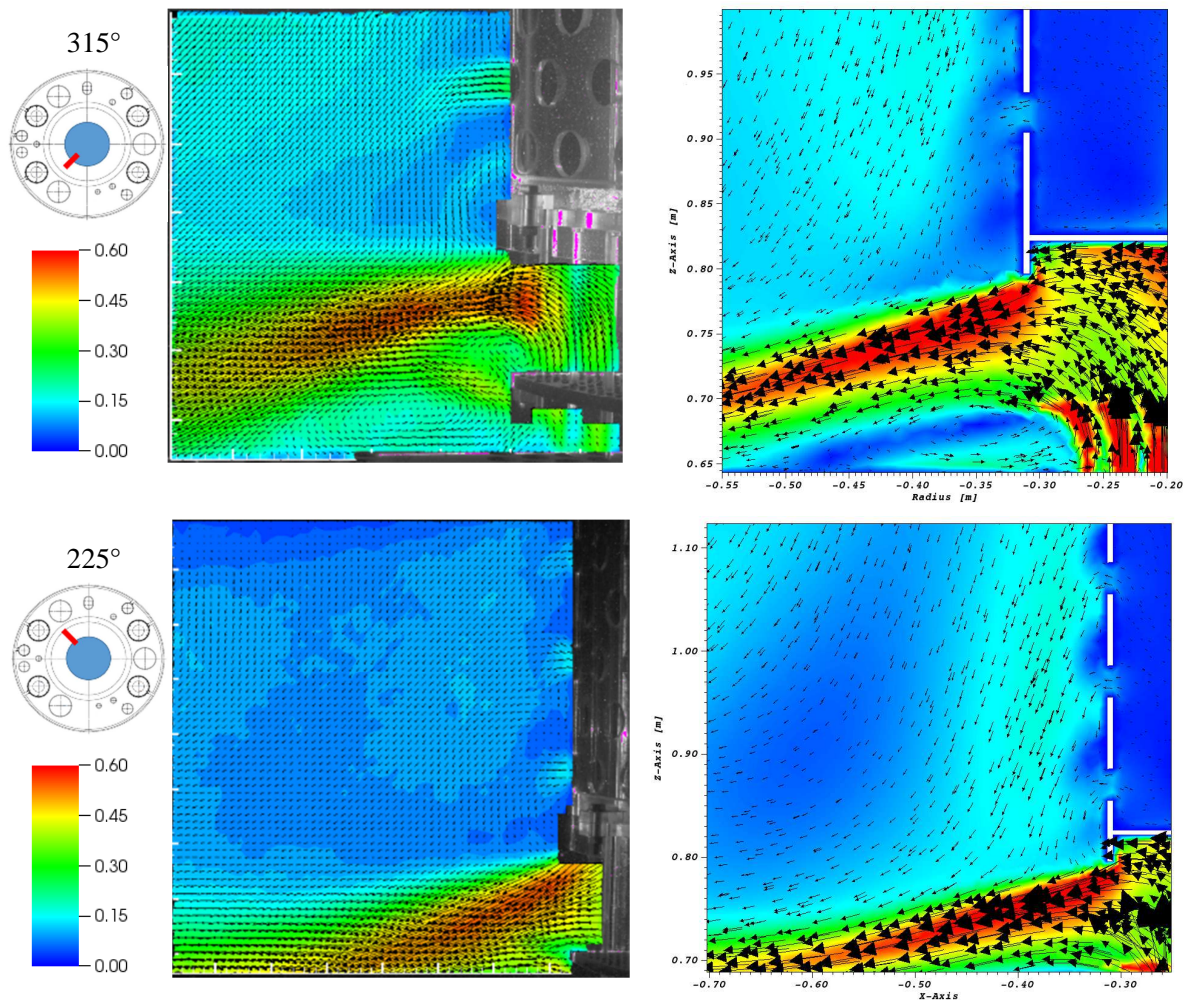
Fig.7: Comparison of measured velocity vectors (left side) to calculated vectors, which are projected on a tetrahedral mesh (center) and on a plane (right side)

### 5.2.2.2 Flow close to the Upper Core Structure

Three experimental planes, which are located normal to the UCS surface and close to the core outlet, were selected to compare quantitatively measurement and calculation. The planes are located at azimuthal angles of  $47^\circ$ ,  $225^\circ$  and  $315^\circ$ . The comparison is shown in Fig.8 by means of 2D vector plots, which have been deduced from the 3D flow field as described above. The experimental results are shown on the left side of Fig.8 and the corresponding calculated results are located on the right side. The vectors show the flow direction and the color scale shows the magnitude of the vectors. The same color maps are used for experiment and calculation.

Most of the flow features already presented in Figs. 5 and 6 are calculated in accordance to the experiment. The flow leaving the core is deflected on the bottom grid and the barrel bottom plate by about  $105^\circ$  from the vertical axis. The locations of bottom grid and barrel bottom plate are added to the left figure of Fig 7. The calculation predicts well the deflection angle with maximum horizontal velocities of about 0.6 m/s. Likewise, the formation of large circulation zones in the hot pool (also shown in Fig.5) and the presence of horizontal jets leaving the UCS by the cylindrical barrel holes (location see Fig.7) are well

predicted. The circulation velocity is slightly overestimated in the calculation, but then again the flow direction is correct. The small recirculation zones, measured above the edge of the bottom grid, cannot be reproduced by the calculation, since the bottom grid is modelled by a singular pressure loss. A strong dependency of the velocity of deflected jet on small changes of the azimuthal angle has been observed in Fig.4. Hence, it is not evident to achieve a better accordance between measurement and calculation.



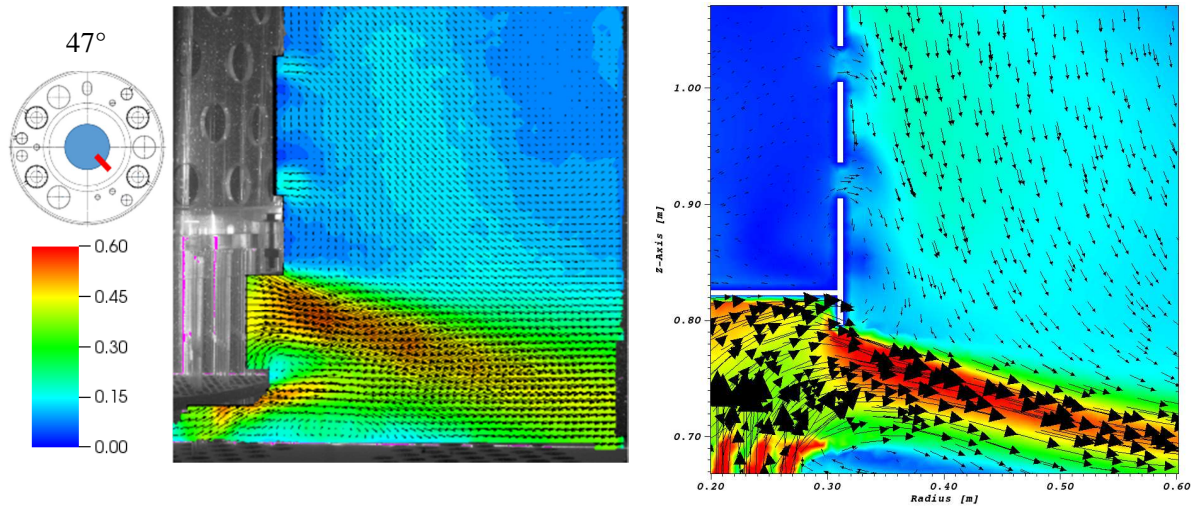
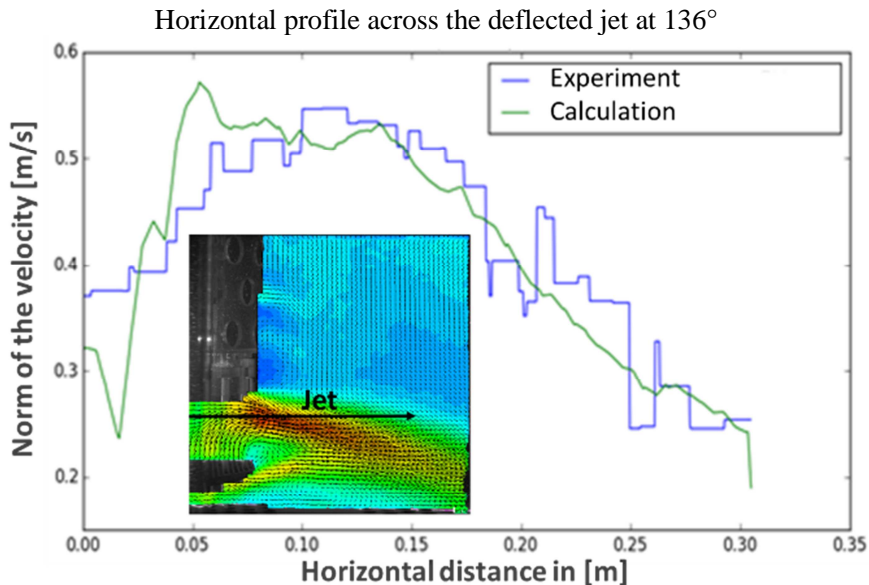


Fig.8: Comparison of measured (left) and calculated (right) velocity fields at the azimuthal angles of 315° (top figures), 225° (center figures) and 47° (lower figures).

A further quantitative comparison of horizontal profiles of the magnitude (norm) of the velocity is shown in Fig.9. The comparison is performed for the measuring plane at 136° (see Fig.2). The profiles are located vertically between core outlet and UCS and point horizontally in direction normal to the UCS cylindrical barrel. Location and orientation of the profiles in the measuring plane are shown schematically in the figures. Two measured and calculated profiles are compared; one directed across the deflected jet and one close above to the bottom grid. The experimental curves show a stepwise profile, the measured values are located in the center of each step. The profiles of the norm of the velocity across the jet (top figure) show a very good agreement. Close to the bottom grid (bottom figure), the effect of the holes in the plate are visible in the experimental values. Above the solid part of the grid, between the holes, the velocity drops to very small values.



Horizontal profile above the bottom grid at 136°

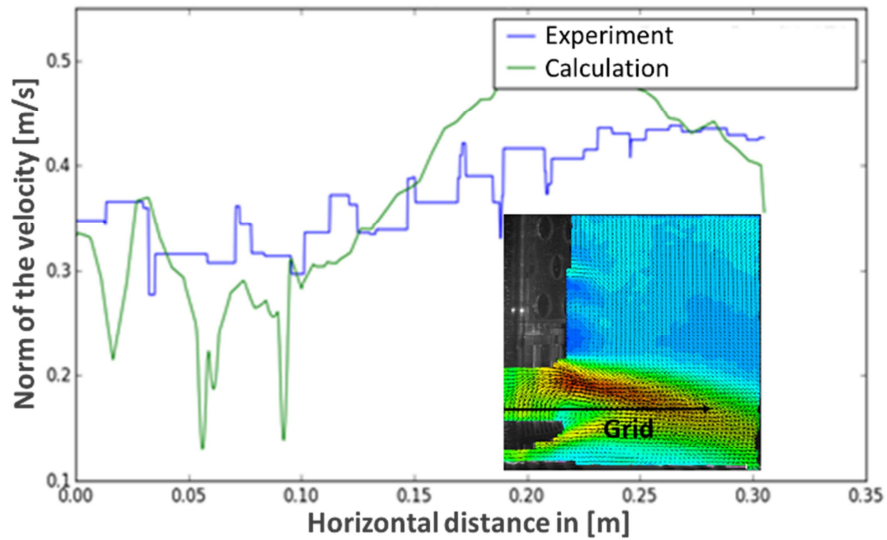


Fig.9: Comparison of measured and calculated horizontal profiles in radial direction of the norm of the velocity in a vertical plane at 136°; across the jet (top figure) and above the bottom grid (bottom figure)

This effect cannot be represented in the calculation by using a porous medium approach for simulating the bottom grid. It seems to be important in further advanced studies to add the bottom grid to the CAD model in order to avoid the homogenization of the flow, which also avoids the formation of recirculation zones in the periphery of the grid as shown in Fig.8. Nevertheless, the overall agreement between experiment and calculation is good.

### 5.2.2.3 Flow close to the Intermediate Heat Exchangers

Measured and calculated velocity fields close to the IHXs are presented in Fig.10; measurements on the left side of Fig.10 and calculations on the right side. The PIV measurements in two planes close to the inlet plenum of the intermediate heat exchanger IHX1 (see Fig.2) are compared to the corresponding calculation result. The plane in the upper figures spans vertically the space between IHX1 and the main pump P01. The plane in the lower figures is located between IHX1 and the direct heat exchanger DHX1. The vectors show the flow direction in the plane and the color scale shows the magnitude of the vectors. The magnitude of the velocity is shown with the same color map for experiment and calculation.

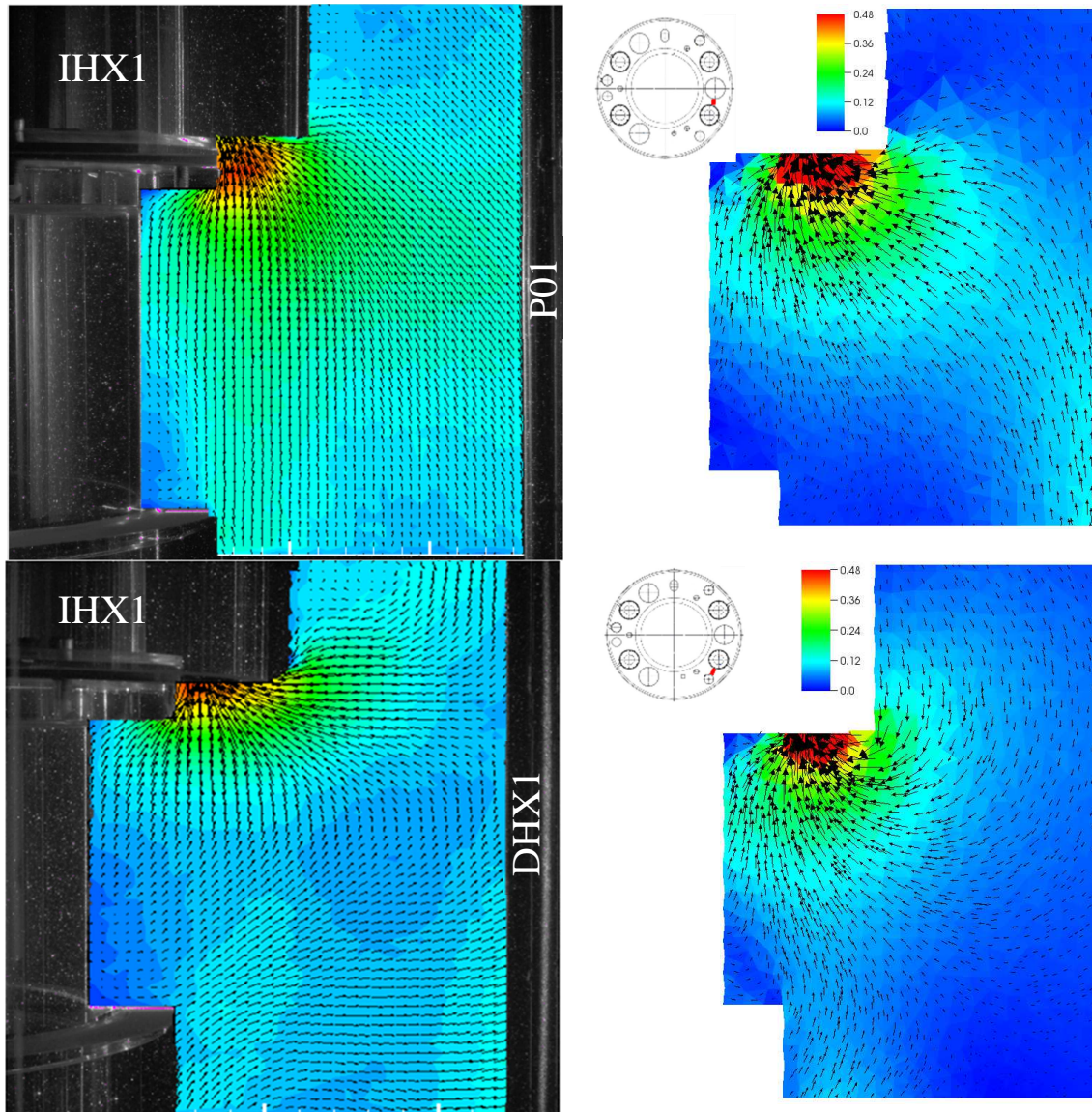


Fig.10: Comparison of measured and calculated velocity fields in vertical planes between IHX1 and P01 (left figure) as well as between IHX1 and DHX1 (right figure)

The flow between IHX1 and P01 is mainly upward directed without a significant aspiration from the zone above the IHX inlet. The flow between IHX1 and DHX1 is upward directed below the IHX inlet with a significant intake from above the IHX inlet. These main flow directions are calculated correctly although differences are present between measured and calculated velocity fields. As already mentioned above, it is difficult to get better accordance between measurement and calculation since a strong dependency exists of the flow field on small changes of the azimuthal angle. The uncertainty of this angle is important since the location of the experimental planes cannot be measured very precisely.

A further quantitative comparison of horizontal and vertical profiles of the norm of the velocity is shown in Fig.11. The comparison is performed for a measuring plane that is located between IHX3 and P02 (see Fig.2). The profiles are situated below the IHX intake; one profile points horizontally in direction to pump P02, one profile is directed downwards, in parallel to the IHX axis. Location and orientation of the profiles in the measuring plane are shown schematically in the figures. As described for Fig. 9, the

experimental curves show a stepwise profile. The horizontal profiles of the norm of the velocity (top figure) show differences between experiment and calculation; the maximal value of the velocity is underestimated and the minimal value is overestimated. Nevertheless, for the first 0.06 m, the decrease of the velocity with increasing distance from the IHX intake is calculated in accordance with the experiment. It seems that one of the profiles is shifted horizontally. The vertical profiles of the norm of the velocity (bottom figure) show a good agreement between experiment and calculation; both the maximum velocity and the decrease of the velocity with increasing distance from the IHX intake are calculated correctly

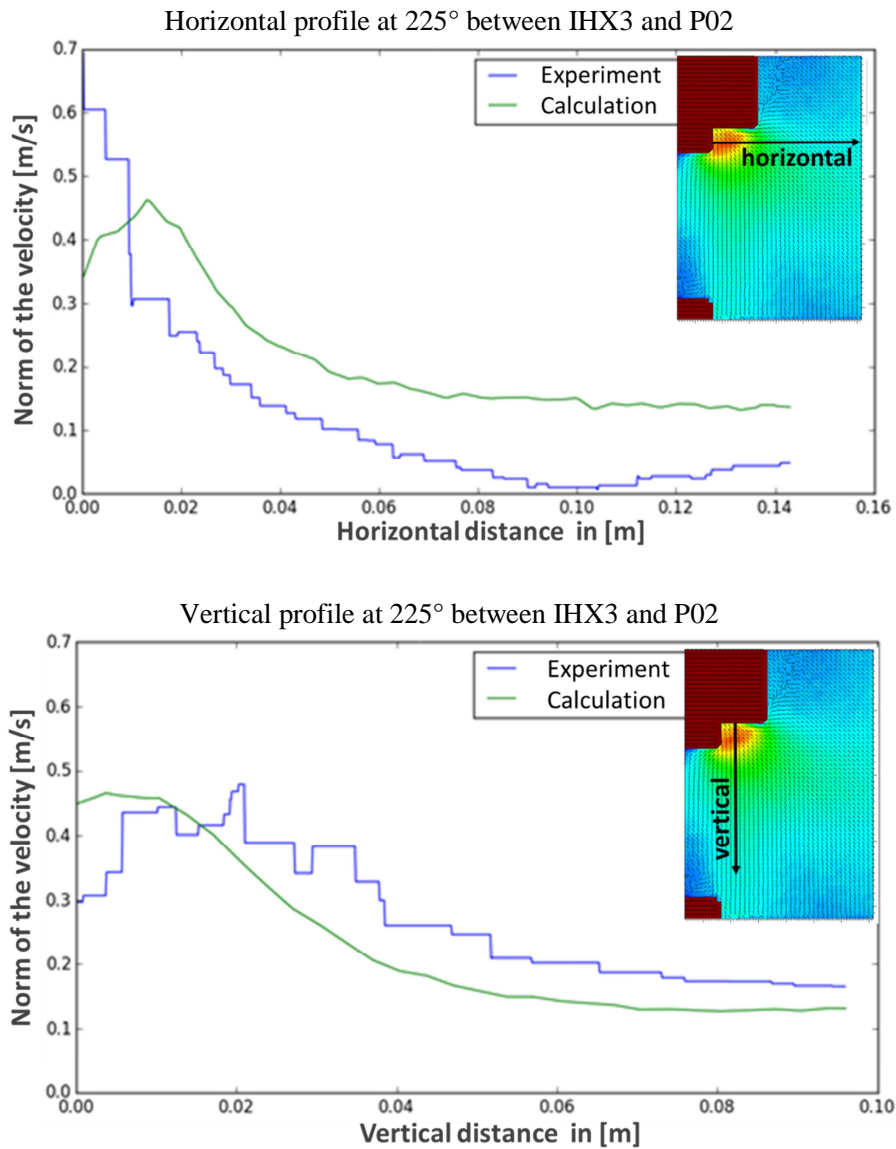


Fig.11: Comparison of measured and calculated profiles of the norm of the velocity in the plane at 225° between IHX3 and P02; horizontal profile (top figure) and vertical profile (bottom figure)

## 6. CONCLUSION

The flow in the MICAS facility is analyzed with the CEA in-house code TrioCFD. MICAS is a 1/6 scale water mockup of the hot pool of the 4<sup>th</sup> generation SFR reactor ASTRID. Detailed information on the test

facility and the experimental setup is given. The use of HPC (High Performance Computing) allows the access to flow fields in complex geometrical structures with a high resolution in space. The numerical model is presented in detail, which has defined based on previously established BPG applicable to the RANS turbulence modelling approach (high Re k- $\epsilon$  model with wall functions). The selection criteria for mesh refinement, numerical schemes and solution procedure are discussed in detail. Based on the guidelines for the meshing, a fine mesh of 28 million tetrahedrons of similar size was created for which steady state solutions have been achieved.

The validation of the modelling approach is shown on the example of one MICAS experiment by comparing calculation results (3D velocity fields) to PIV measurements (2D velocity field). A four step procedure is presented to project the calculation results on the planes of the PIV measurements.

The comparison between measurement and calculation is performed for different locations in the MICAS facility: three vertical planes at different angles around the UCS and two vertical planes close to the IHX1 inlet plenum. A global accordance of the temporal mean velocity is achieved for the overall flow distribution in MICAS. This is true for both locations, the flow close to the UCS and the flow close to the IHX1. **Additionally, selected measured and calculated velocity profiles near the UCS and the IHX3 are compared quantitatively with success. Nevertheless, differences exist locally due to the complexity of the flow topology in the hot pool. In fact, small deviations of the angular direction of an analyzed plane can lead to significant local variations in the velocity field.**

In future advanced analyses, it is planned to add the bottom grid to the CAD model in order to avoid at this location the use of pressure loss modelling and **to improve of the actual turbulence modelling strategy. Further, the comparison of measured and calculated temperature fields will be included in the analysis and the risk of gas entrainment into the IHX will be estimated.**

## ACKNOWLEDGEMENT

This work was granted access to the HPC resources of CINES under the allocation A0032A07571 made by GENCI. Attributed bonus hours were used for this study.

## REFERENCES

- P. Alphonse, J-L. Perrin, P. Gama, “Status of ASTRID architecture and pre-conceptual design”, *Proceedings of Fast Reactors and Related Fuel Cycles (FR13)*, Paris, March 4-7 (2013)
- P.-E. Angeli, U. Bieder U., G. Fauchet, “Overview of the Trio\_U code: Main features, V&V procedures and typical applications to engineering”, *Proceedings of the 16th International Topical Meeting on Nuclear Reactor Thermal Hydraulics (NURTEH16)*, Chicago, Illinois, August 30-September 4 (2015)
- P.-E. Angeli, M.-A. Puscas, G. Fauchet and A. Cartalade, “FVCA8 Benchmark for the Stokes and Navier–Stokes Equations with the TrioCFD Code—Benchmark Session”. In: “Finite Volumes for Complex Applications VIII - Methods and Theoretical Aspects”, *Springer Verlag*, pp.181-202 (2017)
- T. Beck, V. Blanc, J.M. Esclaine, D. Haubensack, M. Pelletier, M. Phelip, B. Perrin and C. Venard “Conceptual design of ASTRID fuel sub-assemblies” *Nucl. Eng. and Design* 315, 51–60 (2017)
- U. Bieder, G.Ziskind, A. Rashkovan, “CFD analysis and experimental validation of steady state mixed convection Sodium flow”. *Nucl. Eng. and Design*, 326C, 333-343 (2018)
- U. Bieder, G. Fauchet, “Analysis of the Natural Convection Flow in the Upper Plenum of the MONJU reactor with TrioCFD” *Science and Technology of Nuclear Installations*, Volume 2013, Article ID 987197

- U. Bieder, “Analysis of the flow down- and upwind of split type mixing vanes”. OCDE workshop CFD4NRS-4, Daejeon, South Korea, 10-12 September (2012)
- M. Crouzieux, P.A. Raviart “Conforming and non-conforming finite element methods for the stationary Stokes equations”. *R.A.I.R.O Anal. Numer.* vol. 7, 33-76 (1973)
- F. Ducros, U. Bieder, O. Cioni, T. Fortin, B. Fournier, G. Fauchet, P. Quéméré “Verification and Validation Considerations regarding the Qualification of numerical schemes for LES for Dilution Problems”. *Nucl. Eng. Design* 240(9), pp 2123–2130 (2010)
- P. Dufour, C. Latge, L Gicquel, “Knowledge passing on in France in the perspective of ASTRID realization”, *Proceedings of Fast Reactors and Related Fuel Cycles (FR13)*, Paris, March 4-7 (2013).
- Q. Feng, U. Bieder, Th. Höhne, “Analysis of Buoyancy-Driven Flow in the ROCOM Test Facility”. *Energy Procedia*, 127, 44-53 (2017)
- A. Gerschenfeld, S. Li, Y. Gorsse, R. Lavastre, “Development and Validation of Multi-Scale Thermal-Hydraulics Calculation Schemes for SFR Applications at CEA” *International Conference on Fast Reactors and Related Fuel Cycles: Next Generation Nuclear Systems for Sustainable Development (FR17)* 26–29 June 2017, Yekaterinburg, Russian Federation
- G Grand, R. Vidil, D. Taillifet and J.P. Benque, “Problèmes posés par la convection mixte du sodium dans les réacteurs rapides; Modélisations physique et numérique“ *LA HOUILLE BLANCHE*, N° 2/3 (1979)
- D. Guenadou, I. Tkatchenko and P. Aubert, “Plateau Facility in Support to Astrid and the SFR Program: An Overview of the First Mock-Up of the Astrid Upper Plenum, MICAS”, *Proceedings of the 16th International Topical Meeting on Nuclear Reactor Thermal Hydraulics (NURTEH16)*, Chicago, Illinois, August 30-September 4 (2015).
- D. Guenadou, P. Aubert, V. Biscay, M. Bottin, J-P. Descamps “Study of the Free Surface Flow in the MICAS Mock-Up in Support of the ASTRID SFR Program”, *Proceedings of the 11th International Topical Meeting on Nuclear Reactor Thermal Hydraulics, Operation and Safety (NUTHOS-11)*, Gyeongju, Korea, October 9-13 (2016).
- D. Guenadou, P. Aubert, V. Biscay and J-P. Descamps, ”Flow analysis in the upper plenum of the MICAS model in support of the ASTRID reactor program. *Proceedings of the 16th International Topical Meeting on Nuclear Reactor Thermal Hydraulics (NURTEH17)*, Xi’an, China, September 3-8 (2017)
- C.V. Hirt, B.D. Nichols, N.C. Romero, “SOLA - A numerical solution algorithm for transient flow”. *Los Alamos National Lab.*, Report LA-5852 (1975)
- H. Hoffmann, “Thermohydraulic investigations of decay heat removal systems by natural convection for liquid-metal fast breeder reactors”. *Nuclear Technology* 88 (1), 75–86 (1989)
- T. Höhne, Kliem S., Bieder U.: IAEA CRP benchmark of ROCOM PTS test case for the use of CFD in reactor design using the CFD-Codes ANSYS CFX and TrioCFD. *Nucl. Eng. Design*, 333, 161-180 (2018)
- IAEA, “Benchmark Analyses of Sodium Natural Convection in the Upper Plenum of the Monju Reactor Vessel” Final Report of a Coordinated Research Project 2008–2012, *IAEA-TECDOC-1754* (2014)
- I.E. Idel’Cik, “Mémento des pertes de charges: Coefficient de pertes de charge singulières et de perte de charge par frottement“, *Direction des études et recherches d'Electricité de France* (1986)
- H. Ohira, Y. Xu, U. Bieder, K. Velusamy, H. Mochizuki, S. Choi, Y. Shvetsov, T. Sofu, J. Thomas, S. Monti, S. Yoshikawa, A. Stanculescu. “Benchmark Analyses of Sodium Natural Convection in the Upper

Plenum of the MONJU Reactor Vessel“ *International Conference on Fast Reactors and Related Fuel Cycles: Safe Technologies and Sustainable Scenarios (FR13)* Paris, France 4-7 March 2013

S. B. Pope, “Turbulent Flows”, *Cambridge University Press*, Cambridge (2000)

A. Rajamania, T. Sundararajana, B.V.S.S.S. Prasada, U. Parthasarathy and K. Velusamy, “Post shut-down decay heat removal from nuclear reactor core by natural convection loops in sodium pool” *Nucl. Eng. Design* 301, 59–73 (2016)

Rakhi, A.K. Sharma and K. Velusamy, “Integrated CFD investigation of heat transfer enhancement using multi-tray core catcher in SFR” *Annals of Nuclear Energy* 104, 256–266 (2017)

H. Reichardt “Vollständige Darstellung der turbulenten Geschwindigkeitsverteilung in glatten Leitungen”. *Zeitschrift für Angewandte Mathematik und Mechanik*, 31, 208 (1951)

D. Tenchine, “Some Thermal Hydraulic Challenges in Sodium Cooled Fast Reactors”, *Nucl. Eng. and Design*, 240, 1195-1217 (2010)

D. Weinberg, K. Rust, H. Hoffmann, Overview report of RAMONA-NEPTUN Program on passive decay heat removal, Forschungszentrum Karlsruhe, *Report FZKA 5667*, 1996